ACS APPLIED MATERIALS & INTERFACES

Research Article

www.acsami.org

High-Efficiency Inverted Polymer Solar Cells with Double Interlayer

Jegadesan Subbiah,[†] Chad M. Amb,[‡] Irfan Irfan,[§] Yongli Gao,*[,§] John R. Reynolds,*[,‡] and Franky So*[,†]

[†]Department of Materials Science and Engineering and [‡]The George and Josephine Butler Polymer Research Laboratory, Department of Chemistry, Center for Macromolecular Science and Engineering, University of Florida, Gainesville, Florida 32611, United States

[§]Department of Physics and Astronomy, University of Rochester, Rochester, New York 14647, United States

ABSTRACT: We have studied the performance of normal and inverted bulk-heterojunction solar cells with an active layer composed of a blend of poly[(4,4′-bis(2-ethylhexyl)dithieno-[3,2-b:2′,3′-d]silole)-2,6-diyl-alt-(2,1,3-benzothiadiazole)-4,7-diyl] (PDTS-BTD) and {6,6}-phenyl-C71 butyric acid methyl ester ($PC_{71}BM$). For inverted cells, a thin layer of ZnO nanoparticles and MoO_3 were used as interlayers for the bottom cathode and the top anode respectively. To enhance the device performance, a thin film of 4,4′,4″-tris[N-(3-methylphenyl)-N-phenylamino]triphenylamine (MTDATA) was used along with MoO_3 as an anode interlayer to improve the hole extraction from the photoactive layer to the anode. The inverted polymer solar cells with double interlayer exhibit a higher power conversion efficiency of 6.45% compared to the conventional cell of 4.91% due to efficient charge extraction and favorable vertical morphology of active layer blend. Our ultraviolet photoemission spectroscopy results indicate that the formation of band bending due to interlayer leads to the enhancement in hole extraction.

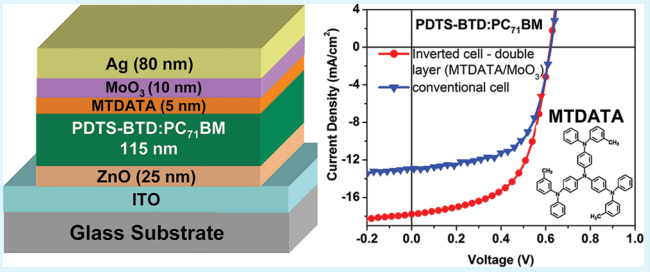

KEYWORDS: *inverted solar cell, photovoltaic, donor−acceptor, bulk heterojunction, conjugated polymers, low bandgap, silole polymer*

1. INTRODUCTION

Organic photovoltaic (OPV) devices have attracted considerable attention as a promising alternative for producing clean and renewable energy because of their potential for low-cost, lightweight, large-area, and flexible solar panels.[1−4] The photoactive layer of polymer solar cells (PSCs) is based on nanoscale networks of bicontinuous donor and acceptor materials, thus providing a large interface area for efficient charge separation and carrier transport.[5−7] Although this large interface exists, the power conversion efficiencies (PCEs) are low to moderate, in part due to inefficient harvesting of the generated charges. Significant efforts have been made to improve the power conversion efficiency (PCE) of PSCs through modifications of interlayer and device architectures.[8−14]

Conventional OPV devices are based on a device structure that consists of an electroactive layer sandwiched between a top low work-function metal cathode and a bottom hole-conducting poly(3,4-ethylenedioxythiophene):poly-(styrenesulfonate) (PEDOT:PSS) layer on top of an indium tin oxide (ITO) coated substrate.[15] However, the strong acidic nature of PEDOT:PSS leads to degradation of the ITO electrode,[16] which impose large problem with respect to device stability and reproducibility of PSCs.[17,18] Efforts have been made to replace the PEDOT:PSS layer by transition metal oxides such as molybdenum oxide (MoO_3), vanadium oxide (V_2O_5) and nickel oxide (NiO) for organic solar cells devices.[19−21] Another problem with the conventional device with a top cathode is oxidation of the low work-function electrodes.[22] An effective approach to solve these problems is to fabricate devices with an inverted geometry where a metal oxide (ZnO or TiO_2) coated ITO acts as the bottom cathode and a high work function metal (Ag or Au) is used as the top anode. In addition, in some material systems such as poly (3-hexylthiophene) (P3HT) deposited with [6,6]-phenyl-C61 butyric acid methyl ester (PCBM), the inverted device architecture has the advantage over the normal geometry due to the vertical phase separation of the active layer where the donor polymer is predominantly at the top of the active layer and the acceptor is at the bottom.[23,24]

In our inverted devices, ZnO nanoparticles are used as an electron transport layer deposited on the bottom of the cell at an ITO contact.[25−28] ZnO has been shown to be a promising electron transporting material with high electron mobility and transparency. For the top p-contact, PEDOT:PSS has been used as the anode interlayer for most inverted cells in the past.[8,29,30] However, spin-coating the PEDOT:PSS layer on top of the electroactive polymer is problematic due to nonuniform wetting on the surface of the active layer.[31] To circumvent this problem, our approach is to use a transition metal oxide interlayer along with a silver electrode to extract holes from the PV cells. Recently, our group and others have demonstrated that MoO_3 can be used as the anode interlayer for efficient hole extraction in polymer solar cells.[21,32−34] Here, we demonstrate

Received: November 4, 2011
Accepted: January 7, 2012
Published: January 7, 2012

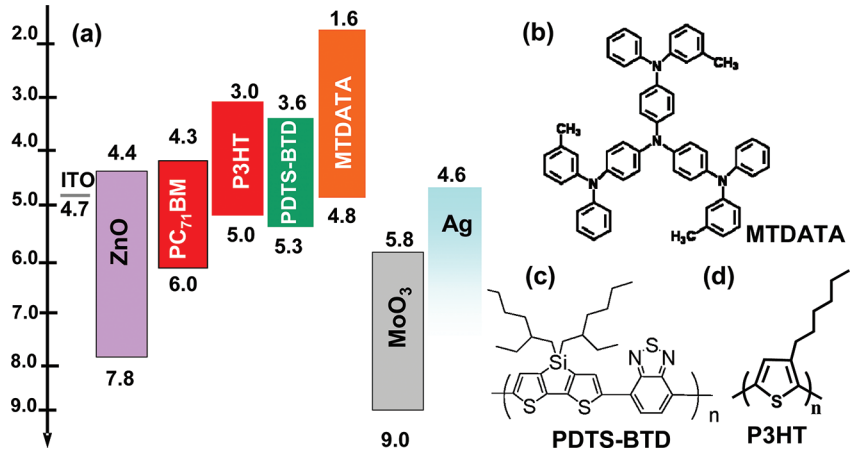

Figure 1. (a) Energy level diagram of the materials used in device fabrication. The molecular structures of (b) small molecule MTDATA, (c) polymers PDTS-BTD, and (d) P3HT.

that an evaporated MoO_3 interlayer can also act as an efficient hole extraction layer in inverted cells. In fact, the inverted cells with a MoO_3 interlayer give higher short-circuit currents than the conventional cells. To further enhance the device performance, we used a thin film of 4,4′,4″-tris[N-(3-methylphenyl)-N-phenylamino]triphenylamine[35] (MTDATA) between the MoO_3 interlayer and the electroactive polymer as an electron blocker. In this work, using this double interlayer approach, inverted bulk-heterojunction solar cells with an active layer composed of a blend of poly[(4,4′-bis(2-ethylhexyl)-dithieno[3,2-b:2′,3′-d]silole)-2,6-diyl-alt-(2,1,3-benzothiadiazole)-4,7-diyl] (PDTS-BTD) and {6,6}-phenyl-C71 butyric acid methyl ester ($PC_{71}BM$) were fabricated. Compared to the conventional device, the inverted cell with the double interlayer substantially enhances the PCE from 4.91% to 6.45%. The enhanced performance of our inverted cells is due to the MoO_3/MTADTA double interlayer, which provides both efficient hole extraction and electron blocking effects. To understand the effect of interlayer, we measured the interface electronic structures of MoO_3/PDTS-BTD and MoO_3/MTADTA/PDTS-BTD using ultraviolet photoemission spectroscopy (UPS) and inverse photoemission spectroscopy (IPES).

2. EXPERIMENTAL DETAILS

Synthesis of ZnO Nanoparticle. ZnO nanoparticles were synthesized from zinc acetate dehydrate and sodium hydroxide (NaOH). The zinc acetate solution was prepared by dissolving zinc acetate dihydrate (0.230 g) in ethanol (15 mL) at 75 °C and the NaOH solution was prepared by dissolving NaOH (0.1 g) in ethanol (5 mL). The NaOH solution was added dropwise to the zinc acetate solution at RT under vigorous stirring. Subsequently, the transparent suspension showed green emission under excitation by an UV lamp. The transparent suspension of nanoparticles was purified by repeated precipitation with heptane, centrifuging and redispersion in EtOH. The washed suspension of ZnO nanoparticles was used for device fabrication.

Vertical Phase Morphology Characterization. The X-ray photoelectron spectroscopy (XPS) data of the active layer top surface were taken directly from the sample surface. In order to investigate the bottom surface of the active layer, the samples were prepared using a lift off technique in which the blended (PDTS-BTD:$PC_{71}BM$) films spin coated on a PEDOT:PSS coated substrate are lifted off from the surface using water and the floated films are transferred to the new substrate with the bottom surface of the layer on the top so that the bottom surface can be measured. To study the vertical profile of PDTS-BTD:$PC_{71}BM$ film, we used a scanning Auger spectroscopy system in combination with Ar-ion-beam milling. The experimental details of the vertical phase morphology have been reported elsewhere.[36]

Device Fabrication. Polymer solar cells were processed on prepatterned indium tin oxide (ITO) coated glass substrates with a sheet resistance of 20 Ω per square. To fabricate conventional PV devices, a thin layer (30 nm) of poly(3,4-ethylenedioxythiophene):poly(styrenesulfonate) (PEDOT:PSS; Baytron AI 4083 from HC Starck) was spin-coated on a ultrasonically cleaned ITO substrates, followed by baking on a hot plate at 180 °C for 10 min. For cells with a MoO_3 interlayer, a thin film (10 nm) of MoO_3 was thermally evaporated on the ITO substrate under a vacuum of 1×10^{-7} Torr. An active layer of the device consisting of the blend of polymer (PDTS-BTD) and $PC_{71}BM$ (1:1.5) was then spin coated from chlorobenzene solvent with a thickness 115 nm. The device was subsequently heated on a hot plate at 150 °C for 5 min. LiF (1 nm) and aluminum (100 nm) were thermally evaporated at a vacuum of 1×10^{-7} Torr on top of active layer as a cathode.

Inverted solar cells were fabricated by spin-coating ZnO nanoparticles on top of the ITO glass substrate and then annealed at 120 °C for 20 min. An active layer solution of PDTS-BTD and $PC_{71}BM$ with a concentration of 20 mg/mL was spin-cast on top of ZnO film followed by annealing of 150 °C for 5 min. For devices with a MTDATA (purchased from Lumtec) interlayer, a 5 nm-thick MTDATA thin film was thermally evaporated on the top of the active layer under a vacuum of 1×10^{-6} Torr. MoO_3 (5 nm) and silver (80 nm) were sequentially evaporated at a vacuum pressure of 1×10^{-7} Torr on top of the active layer as a anode. The device area was 0.04 cm^2. Current density versus voltage measurements were carried out using a Keithley 4200 semiconductor characterization system under AM1.5G solar simulator with an irradiation intensity of 100 mW/cm^2. Device fabrication was done under nitrogen atmosphere and characterizations were performed in an ambient environment without any encapsulation.

Thin Film Characterization. The UPS and IPES studies were performed using a VGESCA Lab system equipped with a He I (21.2 eV) gas discharge lamp as the UV source. The integrated ultrahigh vacuum (UHV) system for UPS measurements consists of an UPS spectrometer chamber integrated with an evaporation chamber. For UPS measurements, samples were transferred directly from the evaporation chamber into the spectrometer chamber without exposing the samples to atmosphere. The details of the system have been published elsewhere.[37,38] Band gaps are determined from our UPS and IPES data from samples prepared under exactly the same conditions.

dx.doi.org/10.1021/am201537p | ACS Appl. Mater. Interfaces 2012, 4, 866–870

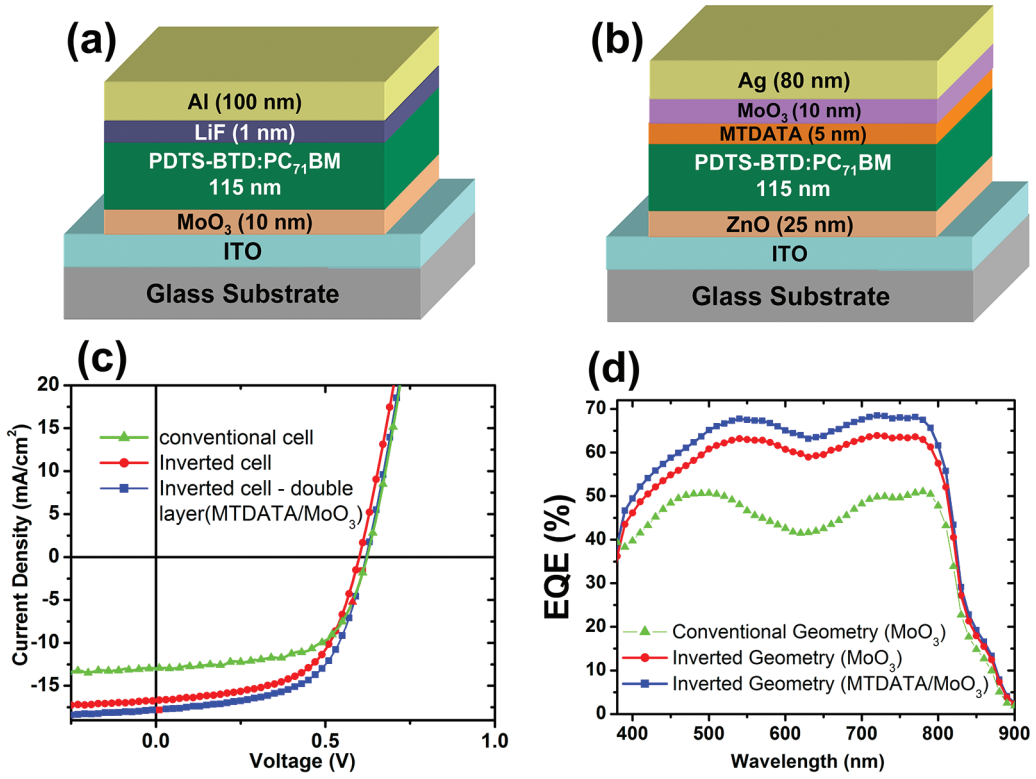

Figure 2. (a) Schematic diagram of PDTS-BTD polymer solar cells with (a) conventional and (b) inverted geometry. (c) $J-V$ curves and (d) EQE of the PDTS-BTD:$PC_{71}BM$-based BHJ solar cells with conventional and inverted geometry under 1.5 solar illumination, 100 mW cm^{-2}.

3. RESULTS AND DISCUSSION

The energy levels of various components used in the solar cells along with the molecular structures of PDTS-BTD, P3HT and MTDATA are shown in Figure 1 as determined from UPS measurements. The details of the ZnO nanoparticle synthesis and device fabrication are described in the Experimental Section. The polymer PDTS-BTD was synthesized according to a previously reported method.[39] The schematic diagrams of both conventional and inverted devices are shown in panels a and b in Figure 2, respectively. Table 1 summarizes the performance characteristics of solar cell devices under 1 sun illumination where the performance of the inverted solar cells is compared with those constructed using the conventional geometry. The current density–voltage ($J-V$) characteristics of these PV devices are shown in Figure 2c. The conventional PDTS-BTD:$PC_{71}BM$ PV cell has a PCE of 4.91%, a short-circuit current density (J_{sc}) of 12.97 mA/cm^2, an open-circuit voltage (V_{oc}) of 0.62 V and a fill factor (FF) of 0.61. Upon changing to an inverted cell design with a MoO_3 interlayer between the photoactive layer and the silver (Ag) anode, the device performance is significantly enhanced, with the PCE being elevated from 4.91 to 5.81%. The major enhancement is the large increase in J_{sc}, from 12.97 to 16.77 mA/cm^2, with little change in the V_{oc} and FF. Here, the enhancement in device performance is attributed to the favorable vertical morphology which provides efficient charge extraction pathways and lower charge recombination.[23] We have studied the vertical morphology of the active layer using X-ray photoelectron spectroscopy. The results show that the top surface is sulfur-rich while the bottom surface is carbon-rich indicating that the top surface of the blend is polymer-rich and the bottom surface is fullerene-rich. Our Auger electron spectroscopy depth profiling data also confirm this vertical phase morphology.[36] This morphology is more favorable for inverted devices which collect holes at the top electrode and electrons at the bottom transparent electrode.

Table 1. Photovoltaic Performance Characteristics of PDTS-BTD:$PC_{71}BM$ Solar Cell with Different Device Geometry

device geometry	J_{sc} (mA/cm^2)	V_{oc} (V)	FF (%)	PCE (%)
conventional	12.97	0.62	61	4.91
inverted	16.77	0.60	59	5.81
inverted – double interlayer	17.81	0.61	59	6.45

The inverted device performance was further enhanced with a double interlayer (MoO_3 + MTDATA) and the corresponding cell has a J_{SC} of 17.81 mA/cm^2, a V_{OC} of 0.61 V and a FF of 59%, resulting in a PCE of 6.45% (Table 1), which corresponds to a 31% increase in the PCE when compared to the conventional cell. The PCE was typically derived from the average of 24 pixels. We had previously used a similar double interlayer strategy in conventional devices, employing poly(9,9-dioctylfluorene-*co*-N-[4-(3-methylpropyl)]-diphenylamine) (TFB) as a bottom electron blocking layer on top of an ITO/MoO_3 layer.[40] Here, we also attempted to use the solution processable TFB as an electron blocking layer in the inverted devices shown here, however the solvent for TFB partially dissolved the underlying electroactive layer and hence reduced the device performance, whereas the vacuum-deposited MTDATA interlayer enhanced it significantly.

The external quantum efficiencies (EQEs) of the devices with the conventional and inverted device geometries are shown in Figure 2d, where all devices show broad optical absorption between 400 and 800 nm. For the inverted cell with a double interlayer (MoO_3+MTDATA), the maximum EQE is

68% at 720 nm, whereas the EQE of the conventional cell is 50%. These results further demonstrate the enhancement in the device performance due to the combined effect of the double interlayer as well as the inverted device geometry.

To explore the general nature of the effect of MTDATA, we studied the double interlayer (MoO_3+MTDATA) effect on the performance of photovoltaic cells employing P3HT: $PC_{71}BM$ blend as an active layer. The $J-V$ characteristics of the P3HT:$PC_{71}BM$ devices with conventional and inverted geometry are shown in Figure 3 and the performance of the

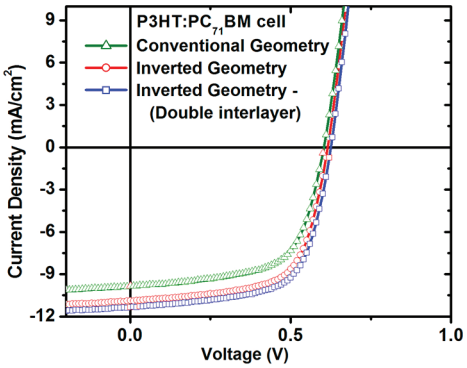

Figure 3. $J-V$ curves of a P3HT:$PC_{71}BM$ solar cells with conventional and inverted architecture.

Table 2. Summary of Performance Parameters of P3HT:$PC_{71}BM$ Solar Cells with Different Device Geometry

device geometry	J_{sc} (mA/cm^2)	V_{oc} (V)	*FF* (%)	PCE (%)
Conventional	9.84	0.60	65	3.80
Inverted	10.88	0.61	66	4.36
Inverted – double interlayer	11.33	0.62	66	4.62

PV devices is summarized in Table 2. The device data show a similar enhancement in device performance due to an increase in short-circuit current in the inverted cell with a double interlayer. The PV cell (P3HT:$PC_{71}BM$) with a conventional geometry shows a PCE of 3.80%, whereas the inverted PV cell with a double interlayer (MoO_3+MTDATA) shows a PCE of 4.62%.

Considering the shallow LUMO energy (1.6 eV) of the MTDATA layer (Figure 1), we expect it to be an effective electron blocker which gives rise to the enhanced performance of the double interlayer cells. It should be noted that the MTDATA layer can act as an exciton blocker here. However, because of the small exciton diffusion length, the effect of exciton blocking on device performance is expected to be small.

To further understand the enhanced performance due to the double interlayer, we studied the energetics of the MoO_3/MTDATA interlayer using UPS and IPES. From the UPS and IPES data, the energy level alignment diagrams for MoO_3 on PDTS-BTD+$PC_{71}BM$, and MoO_3 on MTDATA/PDTS-BTD +$PC_{71}BM$ interfaces were obtained and the data are presented in panels a and b in Figure 4, respectively. From Figure 4a, the vauum level and highest occupied molecular orbital (HOMO) onset for PDTS-BTD blended with $PC_{71}BM$ were measured to be 4.10 and 0.51 eV away from the Fermi level, respectively. Upon deposition of MoO_3 on PDTS-BTD+$PC_{71}BM$, a shift of 0.5 eV in HOMO energy and vacuum level toward the lower

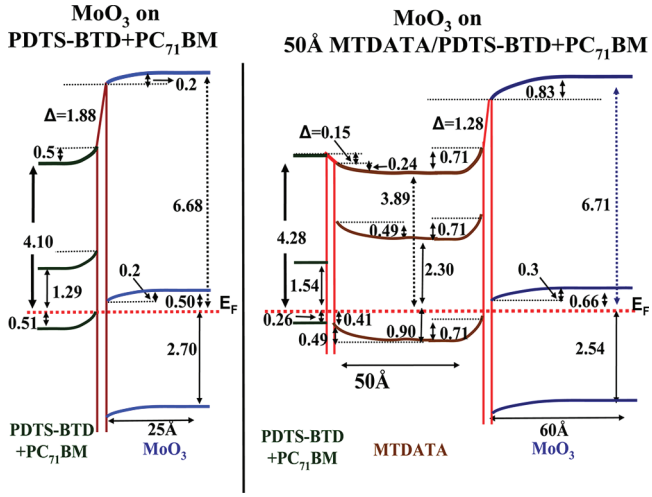

Figure 4. Energy level alignment at (a) PDTS-BTD:$PC_{71}BM$/MoO_3 and (b) PDTS-BTD:$PC_{71}BM$/MTDATA/MoO_3.

binding energy (BE) was observed. This shift is due to the transfer of electrons from the polymer to MoO_3.[34] Because the HOMO onset was 0.51 eV below the Fermi level, the 0.5 eV shift in the vacuum level renders the HOMO level pinned at the Fermi level. On the other hand, a smaller shift of 0.2 eV was observed in the valence level of MoO_3 with deposition of MoO_3 on the PDTS-BTD+$PC_{71}BM$ film, which almost saturated with 11 Å of MoO_3 deposited. The interface dipole at the MoO_3/PDTS-BTD+$PC_{71}BM$ interface was measured to be 1.88 eV. The work function (WF) and HOMO onset of MoO_3 (at a thickness of 26 Å) were measured to be 6.68, and 2.70 eV, respectively. Here, our results show that the band-bending of the PDTS-BTD HOMO level leads to an enhancement in hole extraction, which is consistent with our previous work.[21,37]

To study the double interlayer effects, we deposited MTDATA layer by layer on the PDTS-BTD+$PC_{71}BM$ film and monitored by UPS and IPES. The HOMO onset values gradually shifted from 0.41 to 0.90 eV as the thickness of the MTDATA layer increases from 5 to 50 Å, giving rise to a band bending of 0.49 eV in MTDATA (Figure 4b). The WF was measured to be 3.89 eV for a 50 Å thick MTDATA. MoO_3 was then deposited layer by layer on the MTDATA/PDTS-BTD +$PC_{71}BM$ film. With increasing MoO_3 thickness, the MTDATA HOMO onset values gradually shift toward the lower BE. This shift was measured to be 0.71 eV. The valence band peak of MoO_3 was also observed to be gradually shifting toward the lower BE and this shift was measured to be 0.3 eV. The interface dipole was measured to be 1.28 eV between the MoO_3 /MTDATA interface. The WF and valence band edge for a 64 Å thick MoO_3, were measured to be 6.71, and 2.54 eV, respectively. The HOMO–LUMO gaps of PDTS-BTD +$PC_{71}BM$, and MTDATA were measured to be 1.8, and 3.2 eV, respectively. The energy level diagram (Figure 4) suggests that the MoO_3 interlayer substantially improves hole extraction due to band bending at the interface and, thus, giving rise to higher J_{sc} which in turn enhances the device performance. The MTDATA interlayer between active layer and the MoO_3 interlayer acts as an electron blocking layer by imposing an energetically inaccessible conduction band at the interface, which further increases the overall short-circuit current.

dx.doi.org/10.1021/am201537p | ACS Appl. Mater. Interfaces 2012, 4, 866–870

4. CONCLUSION

We have demonstrated that inverted geometry PDTS-BTD polymer cells with a double interlayer showed a 31% enhancement in power conversion efficiency when compared with a conventional cell with a bottom p-contact. The enhanced device performance is attributed to the combined effect of favorable vertical phase separation of the active layer for the inverted architecture, along with effective electron blocking/charge extraction due to the double interlayer. Our results show that that interface materials and device geometry are important parameters for achieving high-performance polymer solar cells.

AUTHOR INFORMATION

Corresponding Author

*E-mail: fso@mse.ufl.edu (F.S.); reynolds@chem.ufl.edu (J.R.R.); yongli.gao@rochester.edu (Y.G.).

ACKNOWLEDGMENTS

The authors gratefully acknowledge the financial support from Sestar, the Florida Energy Systems Consortium and the Air Force Office of Scientific Research (FA9550-09-1-0320).

REFERENCES

(1) Gunes, S.; Neugebauer, H.; Sariciftci, N. S. *Chem. Rev.* **2007**, *107*, 1324−1338.
(2) Dennler, G.; Scharber, M. C.; Brabec, C. J. *Adv. Mater.* **2009**, *21*, 1323−1338.
(3) Thompson, B. C.; Fréchet, J. M. J. *Angew. Chem., Int. Ed.* **2008**, *47*, 58−77.
(4) Krebs, F. C. *Sol. Energy Mater. Sol. Cells* **2009**, *93*, 394−412.
(5) Li, G.; Shrotriya, V.; Huang, J. S.; Yao, Y.; Moriarty, T.; Emery, K.; Yang, Y. *Nat. Mater.* **2005**, *4*, 864−868.
(6) Liang, Y.; Xu, Z.; Xia, J.; Tsai, S.-T.; Wu, Y.; Li, G.; Ray, C.; Yu, L. *Adv. Mater.* **2010**, *22*, E135−E138.
(7) Wienk, M. M.; Turbiez, M.; Gilot, J.; Janssen, R. A. J. *Adv. Mater.* **2008**, *20*, 2556−2560.
(8) Hau, S. K.; Yip, H.-L.; Baek, N. S.; Zou, J.; O'Malley, K.; Jen, A. K. Y. *Appl. Phys. Lett.* **2008**, *92*, 253301.
(9) Peet, J.; Kim, J. Y.; Coates, N. E.; Ma, W. L.; Moses, D.; Heeger, A. J.; Bazan, G. C. *Nat. Mater.* **2007**, *6*, 497−500.
(10) Chu, T.-Y.; Lu, J.; Beaupreì, S.; Zhang, Y.; Pouliot, J.-R. m.; Wakim, S.; Zhou, J.; Leclerc, M.; Li, Z.; Ding, J.; Tao, Y. *J. Am. Chem. Soc.* **2011**, *133*, 4250−4253.
(11) Subbiah, J.; Beaujuge, P. M.; Choudhury, K. R.; Ellinger, S.; Reynolds, J. R.; So, F. *Org. Electron.* **2010**, *11*, 955−958.
(12) Li, G.; Yao, Y.; Yang, H.; Shrotriya, V.; Yang, G.; Yang, Y. *Adv. Funct. Mater.* **2007**, *17*, 1636−1644.
(13) Kim, J. Y.; Lee, K.; Coates, N. E.; Moses, D.; Nguyen, T.-Q.; Dante, M.; Heeger, A. J. *Science* **2007**, *317*, 222.
(14) Alexander, W. H.; Tobin, J. M. *Appl. Phys. Lett.* **2008**, *92*, 023504.
(15) Ma, W.; Yang, C.; Gong, X.; Lee, K.; Heeger, A. J. *Adv. Funct. Mater.* **2005**, *15*, 1617−1622.
(16) Yan, H.; Lee, P.; Armstrong, N. R.; Graham, A.; Evmenenko, G. A.; Dutta, P.; Marks, T. J. *J. Am. Chem. Soc.* **2005**, *127*, 3172−3183.
(17) Norrman, K.; Madsen, M. V.; Gevorgyan, S. A.; Krebs, F. C. *J. Am. Chem. Soc.* **2010**, *132*, 16883−16892.
(18) Norrman, K.; Gevorgyan, S. A.; Krebs, F. C. *ACS Appl. Mater. Interfaces* **2009**, *1*, 102−112.
(19) Irwin, M. D.; Buchholz, D. B.; Hains, A. W.; Chang, R. P. H; Marks, T. J. *Proc. Natl. Acad. Sci.* **2008**, *105*, 2783−2787.
(20) Shrotriya, V.; Li, G.; Yao, Y.; Chu, C.-W.; Yang, Y. *Appl. Phys. Lett.* **2006**, *88*, 073508.
(21) Kim, D. Y.; Subbiah, J.; Sarasqueta., G.; So, F.; Ding, H.; Irfan.; Gao, Y. *Appl. Phys. Lett.* **2009**, *95*, 093304.
(22) Jørgensen, M.; Norrman, K.; Krebs, F. C. *Sol. Energy Mater. Sol. Cells* **2008**, *92*, 686−714.
(23) Xu, Z.; Chen, L.-M.; Yang, G.; Huang, C.-H.; Hou, J.; Wu, Y.; Li, G.; Hsu, C.-S.; Yang, Y. *Adv. Funct. Mater.* **2009**, *19*, 1227−1234.
(24) Campoy-Quiles, M.; Ferenczi, T.; Agostinelli, T.; Etchegoin, P. G.; Kim, Y.; Anthopoulos, T. D.; Stavrinou, P. N.; Bradley, D. D. C.; Nelson, J. *Nat. Mater.* **2008**, *7*, 158−164.
(25) Yip, H.-L.; Hau, S. K.; Baek, N. S.; Ma, H.; Jen, A. K. Y. *Adv. Mater.* **2008**, *20*, 2376−2382.
(26) Park, M.-H.; Li, J.-H.; Kumar, A.; Li, G.; Yang, Y. *Adv. Funct. Mater.* **2009**, *19*, 1241−1246.
(27) Sun, Y.; Seo, J. H.; Takacs, C. J.; Seifter, J.; Heeger, A. J. *Adv. Mater.* **2011**, *23*, 1679−1683.
(28) Yang, T.; Cai, W.; Qin, D.; Wang, E.; Lan, L.; Gong, X.; Peng, J.; Cao, Y. *J. Phys. Chem. C* **2010**, *114*, 6849−6853.
(29) Rider, D. A.; Worfolk, B. J.; Harris, K. D.; Lalany, A.; Shahbazi, K.; Fleischauer, M. D.; Brett, M. J.; Buriak, J. M. *Adv. Funct. Mater.* **2010**, *20*, 2404−2415.
(30) Hsieh, C.-H.; Cheng, Y.-J.; Li, P.-J.; Chen, C.-H.; Dubosc, M.; Liang, R.-M.; Hsu, C.-S. *J. Am. Chem. Soc.* **2010**, *132*, 4887−4893.
(31) Weickert, J.; Sun, H.; Palumbiny, C.; Hesse, H. C.; Schmidt-Mende, L. *Sol. Energy Mater. Sol. Cells* **2010**, *94*, 2371−2374.
(32) Beaujuge, P. M.; Subbiah, J.; Choudhury, K. R.; Ellinger, S.; McCarley, T. D.; So, F.; Reynolds, J. R. *Chem. Mater.* **2010**, *22*, 2093−2106.
(33) Kröger, M.; Hamwi, S.; Meyer, J.; Riedl, T.; Kowalsky, W.; Kahn, A. *Org. Electron.* **2009**, *10*, 932−938.
(34) Nakayama, Y.; Morii, K.; Suzuki, Y.; Machida, H.; Kera, S.; Ueno, N.; Kitagawa, H.; Noguchi, Y.; Ishii, H. *Adv. Funct. Mater.* **2009**, *19*, 3746−3752.
(35) Adachi, C.; Kwong, R.; Forrest, S. R. *Org. Electron.* **2001**, *2*, 37−43.
(36) Subbiah, J.; Amb, C.; Reynolds, J. R.; So, F. *Sol. Energy Mater. Sol. Cells* **2011**, *97*, 97−101.
(37) Irfan.; Ding, H.; Gao, Y.; Kim, D.; Subbiah, J.; So, F. *Appl. Phys. Lett.* **2010**, *96*, 073304.
(38) Watkins, N. J.; Gao, Y. *J. Appl. Phys.* **2003**, *94*, 5782.
(39) Choudhury, K. R.; Subbiah, J.; Chen, S.; Beaujuge, P. M.; Amb, C. M.; Reynolds, J. R.; So, F. *Sol. Energy Mater. Sol. Cells* **2011**, *95*, 2502−2510.
(40) Subbiah, J.; Kim, D. Y.; Hartel, M.; So, F. *Appl. Phys. Lett.* **2010**, *96*, 063303.